

**EFFECTS OF INTRA- AND INTER-LAMINAR RESIN CONTENT ON
THE MECHANICAL PROPERTIES OF TOUGHENED COMPOSITE MATERIALS¹**

Dodd H. Grande and Larry B. Ilcewicz
Boeing Commercial Airplane Group

William B. Avery
Boeing Defense and Space Group

Willard D. Bascom
University of Utah

54-24
175645

ABSTRACT

Composite materials having multiphase toughened matrix systems and laminate architectures characterized by resin rich interlaminar layers (RIL) have been the subject of much recent attention. Such materials are likely to find applications in thick compressively loaded structure such as the keel area of commercial aircraft fuselages. The effects of resin content and its interlaminar and intralaminar distribution on mechanical properties were investigated with test and analysis for two such carbon/epoxy systems. The RIL was found to reduce the in situ strengthening effect for matrix cracking in laminates. Mode II fracture toughness was found to increase with increasing RIL thickness over the range investigated, and mode I interlaminar toughness was negligibly affected. Compressive failure strains were found to increase with increasing resin content for specimens having no damage, holes, and impact damage. Analytical tools for predicting matrix cracking of off-axis plies and damage tolerance in compression after impact (CAI) were successfully applied to materials with RIL.

INTRODUCTION*

Historically, there has been a general trend towards increased fiber volume fraction in composite materials. For example, some applications favor higher fiber content to maximize fiber dominated properties such as stiffness. Little has been done to investigate optimum resin contents for properties dominated by the matrix (e.g., toughness and compression strength). The keel area in an aircraft fuselage may favor a somewhat higher resin content due to the need for enhanced interlaminar shear load transfer. Important issues for keel applications include (a) impact damage resistance and tolerance, (b) the effect of stress concentrations such as holes and ply drops, and (c) response to compressive loadings.

Control of lamina scale architecture is one route which has been employed in recent years to influence matrix-dominated composite properties. This approach has been used to produce composite laminates having resin rich zones in the interlaminar region. One advantage of such architecture is high damage resistance to shear dominated impact events.

The purpose of this work was to investigate the effects of resin content, and its inter- and intra-laminar distribution on the mechanical performance of toughened epoxy matrix composites. In particular, the effects of resin-rich interlaminar layers (RIL) were examined. A range of mechanical properties were studied. Experimental and analytical studies were performed to determine the effects of an RIL on in situ strengthening and matrix cracking in off-axis plies. The effects of inter- and intra-laminar resin

¹ This work was funded by Contract NAS1-18889, under the direction of J.G. Davis and W.T. Freeman of NASA Langley Research Center.

* [This paper cites references 1--19.]

content on mode I and mode II interlaminar toughness, compressive strength, and impact damage resistance and tolerance were studied experimentally for four batches of materials which were produced with varying inter and intra-laminar resin contents. Analytical models were used to predict the damage tolerance for these materials.

BACKGROUND

It is important to examine the available analytical tools for their applicability to emerging composite forms and architectures. In some cases, such as for matrix cracking in RIL materials, modifications to existing approaches are necessary to adequately predict behavior. Other cases such as damage tolerance of CAI panels may be adequately addressed using current approaches as long as the damage zone is dominated by delaminations or other well understood mechanisms.

Examples of materials which tend to have RIL architectures are American Cyanamid interleaf materials, Hercules IM7/8551-7, and Toray T800/3900-2. The presence of RIL has been shown to influence mode II interlaminar toughness, CAI behavior and matrix cracking in off-axis plies (Refs. 1,2,3). Other cases in which this type of architecture may be important include behavior in the vicinity of ply drops for tape structures and the cured matrix distributions in resin transfer molded parts.

Previous studies have indicated a relationship between compression strength after impact (CAI) and mode II interlaminar toughness test results (Refs. 1,4,5). Increased mode II interlaminar toughness restricts the size of delaminations which form a damage zone comprised of sublaminates (increases damage resistance). The smaller sublaminates lead to higher residual compression strengths. This trend is indicated in Figure 1 showing results for several batches of Hercules IM7/8551-7 studied in earlier work (Ref. 4). It was noted during this work that the batches displaying higher values of CAI also tended to have thicker RIL. Similar observations of the influences of polymeric interlaminar layers on CAI performance have been reported in the literature (Refs. 1,2). Studies using aluminum adherends and controlled adhesive bondlines have shown the effects of adhesive thickness on mode I and mode II toughness (Ref. 6). The mode II toughness was found to increase with increasing adhesive thickness. Similar Results have been reported for studies on composites (Refs. 7,8).

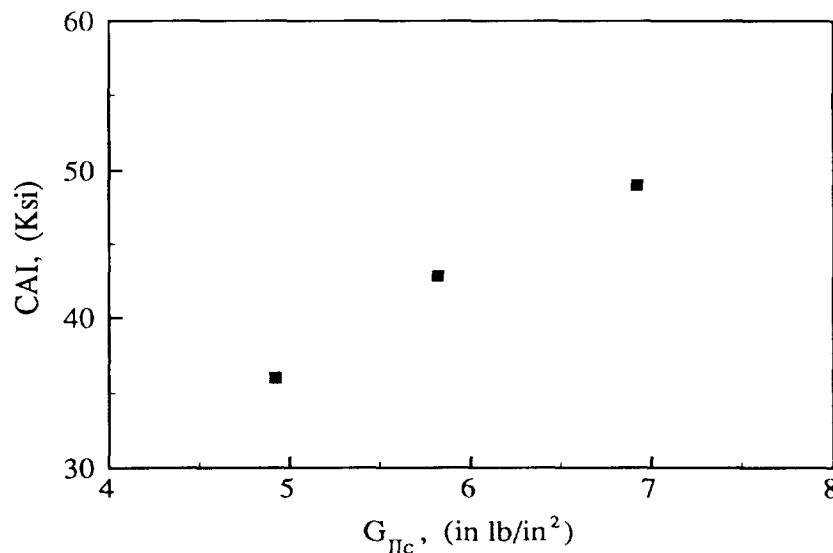


Figure 1. Relationship Between Interlaminar G_{IIc} and CAI.

The residual strength of impact damaged structure is influenced by undamaged compressive strength as well as by the damage which is present (Ref. 9). Analytical studies reported in the literature suggest that ultimate compressive strains may be improved by increased resin content (Refs. 10,11). Verification of such behavior has not been widely reported in the literature.

While the presence of an RIL appears to suppress delamination caused by impact, it has also been found to influence the resistance to matrix cracking in off-axis plies. The presence of relatively compliant RIL reduces the in situ transverse strengthening provided to off-axis plies by neighboring plies. This can result in lower resistance to matrix cracking than would be expected for such toughened materials when neglecting the RIL effect (Ref. 3).

MATERIALS

Materials studied in this work were Hercules IM7/8551-7 and Toray T800/3900-2. Both systems consist of intermediate modulus fibers in toughened multi-phase epoxy matrices, and both systems tend to display RIL architectures. Photomicrographs showing the interlaminar regions of these two materials are given in Figure 2.

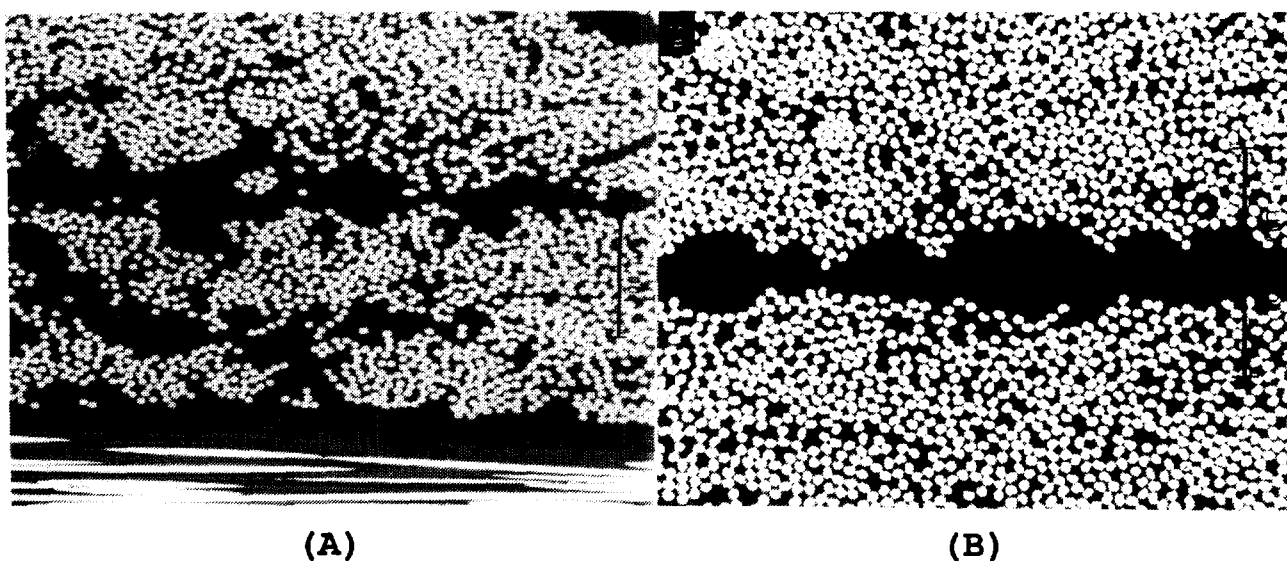


Figure 2. Cross Sections of RIL Microstructure in a.) IM7/8551-7 and b.) T800/3900-2.

A summary of materials used in this study is given in Table 1. Hercules IM7/8551-7 was used as a model RIL material to study matrix cracking in 90 degree plies of multiaxial tensile specimens. Toray T800/3900-2 was used to study the effects of RIL architecture as inter- and intra-laminar resin content were varied. Four batches of Toray materials were obtained in which the inter- and intra-laminar resin contents were systematically varied as given in Table 1. The carbon fiber areal weight was held constant in these studies, so increased resin content also led to increased ply thickness as shown in the Table. The carbon fiber areal weights and resin contents given in Table 1 are the nominal or target

values. Actual experimentally determined values of areal weight and resin content did not vary greatly from these targets. The per ply thicknesses given are typical experimental values from the range of panels fabricated.

MATERIAL	FIBER AREAL WEIGHT (g/m ²)	RESIN CONTENT (% WT)			PLY THICK. (10 ⁻³ in)	FIBER VOLUME (%)
		INTER	INTRA	TOTAL		
IM7/8551-7	190	---	---	35	7.5	0.575
T800/3900-2						
Batch B1	145	Low	Low	35	5.8	0.573
Batch B2	145	Low	High	39	6.3	0.530
Batch B3	145	High	Low	39	6.3	0.530
Batch B4	145	High	High	43	6.9	0.489

Table 1. Material Descriptions

TEST METHODS

Mechanical tests used in this work are listed in Table 2. Specimen stacking sequences and dimensions are given in Table 3. Loadings for all mechanical tests were performed using a servo-hydraulic testing machine. The displacement rate for all tests was 0.05 in/min except as noted below. Displacement rates for interlaminar fracture tests were 1.0 in/min for double cantilever beam and 0.10 in/min for end notch flexure. Impacting was performed on a Dynatup instrumented impact tower. Impact damage area was measured using through transmission ultrasonic inspection (TTU).

PROPERTY	TEST TYPE
Unidirectional Compression Strength	IITRI
Unidirectional Compressive Modulus	Face Supported - Untabbed
Unidirectional Tensile Strength	Tabbed
Mode I Interlaminar Fracture	Double Cantilever Beam
Mode II Interlaminar Fracture	End Notch Flexure
Open Hole Compression	Face Supported
Quasi-isotropic Compression Strength	Face Supported
Compression After Impact	4" X 6" Coupon, 5/8" Dia. Tup
Matrix Cracking	Straight Sided Tabbed Tension
Mode I Intralaminar Fracture	Double Edge Notch

Table 2. Test Methods And Specimen Types

PROPERTY	STACKING SEQUENCE	SPECIMEN DIMENSIONS
Compression Strength	(0) ₁₆	5.5 in. x 0.5 in.
Compressive Modulus	(0) ₈	3.18 in. x 0.5 in.
Tensile Strength	(0) ₈	9 in. x 0.5 in.
Mode I Interlaminar Fracture	(0) ₂₆	13 in. x 0.5 in.
Mode II Interlaminar Fracture	(0) ₂₆	13 in. x 0.5 in.
Open Hole Compression ¹	(+45/0/-45/90) _{2S}	12 in. x 1.5 in.
Open Hole Compression ²	(+45/0/-45/90) _{2S}	12 in. x 2.5 in.
Compression After Impact	(+45/0/-45/90) _{4S}	4 in. x 6 in.
Matrix Cracking	(+45/90 ₂ /-45/0 ₄ /90 ₂) _S	6 in. x 1 in.
Mode I Intralaminar Fracture	(90) ₁₂	12 in. x 1 in.
Notes:	¹ For no hole, 1/8", and 1/4 " diameter holes, face supported. ² For 1/2" diameter hole, face supported.	

Table 3. Specimen Dimensions And Stacking Sequences Used For Mechanical Tests

RESULTS AND DISCUSSIONS

Matrix Cracking Studies

Transverse matrix cracks can occur in composite laminates due to the combined effects of mechanical loading and environment. The transverse strength of a composite ply is not, strictly speaking, a material property as it is strongly influenced by laminate stacking sequence. The influence of neighboring plies on the transverse ply strength is referred to as in situ strengthening. Stiff neighboring plies tend to increase the strains at which matrix cracks develop in off-axis plies due to the crack opening restraint that they provide. The strains for matrix cracking in traditional untoughened materials have been found to decrease with increasing numbers of off-axis plies which are stacked together.

The RIL provides a compliant layer between plies which reduces the constraint provided by neighboring plies. Thus, one of the expected effects of the RIL would be a decrease in the in situ strengthening effect and reduced strains for onset of matrix cracking in off-axis plies for certain stacking sequences. Another influence of the isolation provided by the RIL is to reduce the effect of grouping multiple plies of the same orientation.

Matrix cracking experiments were performed using the IM7/8551-7 material. The lamina architecture of this material tends to exhibit a resin rich zone between adjacent laminae. A photomicrograph showing the RIL in IM7/8551-7 is shown in Figure 2a. The RIL layer was observed to exhibit local variations in thickness, and contains second phase material.

Specimen geometry and stacking sequences were as given in Table 3. Experimental determinations were made of the strain at onset of cracking in the 90° plies at a number of temperatures and humidity conditions. A finite element approach was used to predict the onset of off-axis cracking (Ref. 3). This approach utilizes a crack closure technique to determine the strain energy release rate for cracks in the

90° plies. Mode I intralaminar G_{IC} values were determined using the double edge notch test (Ref. 12). Composite, neat resin and fracture properties used for the analysis were all obtained at the environmental conditions being modelled. Neat resin data were obtained from reference (Ref. 13).

Three different finite element models were constructed to predict onset of matrix cracking in laminates with RIL. The first model ignored RIL architecture and used average ply properties. The second model discretely simulated RIL architecture by concentrating fibers in the central 80% of a ply, with a correspondingly higher local fiber volume fraction. The outer 10% on either side of the ply was modelled as a neat resin layer. Properties of fiber rich regions were scaled to account for increased fiber volume fraction, and RIL were assigned neat resin properties. The third model had the same geometry as the second, with RIL moduli reduced to 25% of the neat resin modulus. The reduced moduli were intended to reflect reductions from bulk stiffness that would be expected due to preferential additions of elastomeric or other modifiers to the RIL layer.

Predicted results from the three models are shown in Figure 3 along with experimental data for the 70°F/dry condition. The figure shows that RIL must be discretely modeled to obtain a good prediction of the onset of matrix cracking. Similar plots for conditions of -75°F/dry and 180°F/wet are shown in Figures 4 and 5. Comparison of these results show that the experimental data fall close to the RIL model using neat resin moduli for the -75°F/dry and 70°F/dry conditions and closest to that using the reduced RIL moduli for the 180°F/wet condition. Reference 3 gives additional experimental and analytical results for matrix cracking in IM7/8551-7.

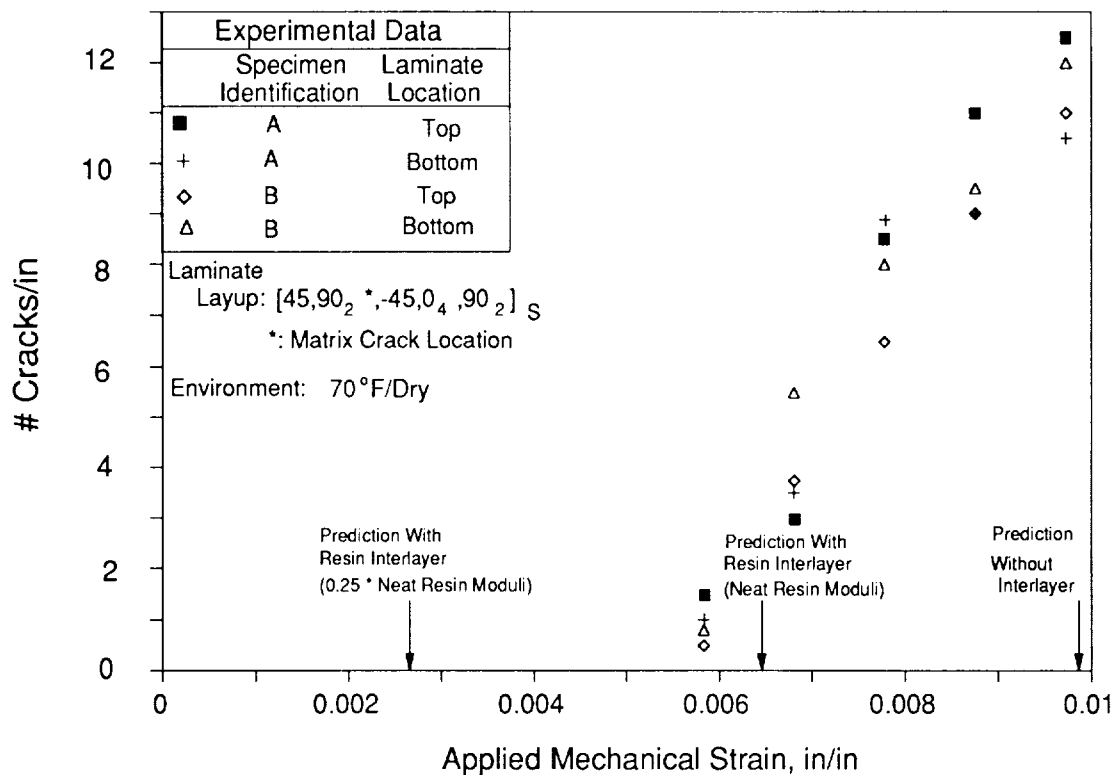


Figure 3. Matrix Crack Onset Predictions and Test Data for a Laminate Exposed to 70°F/Dry.

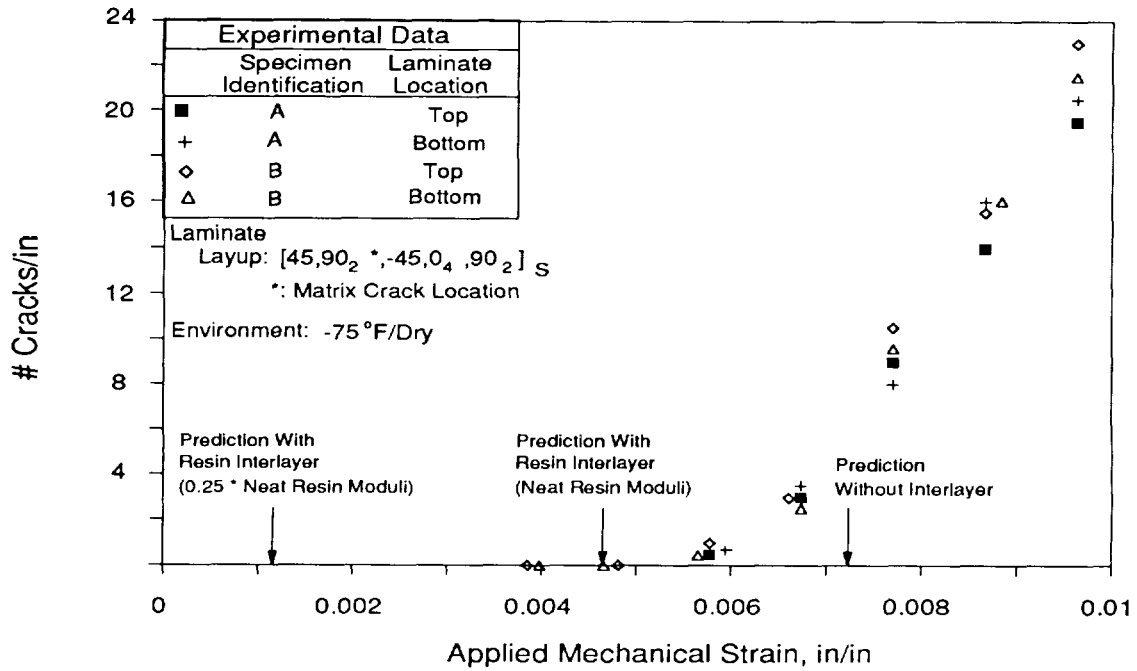


Figure 4. Matrix Crack Onset Predictions and Test Data for a Laminate Exposed to -75°F/Dry.

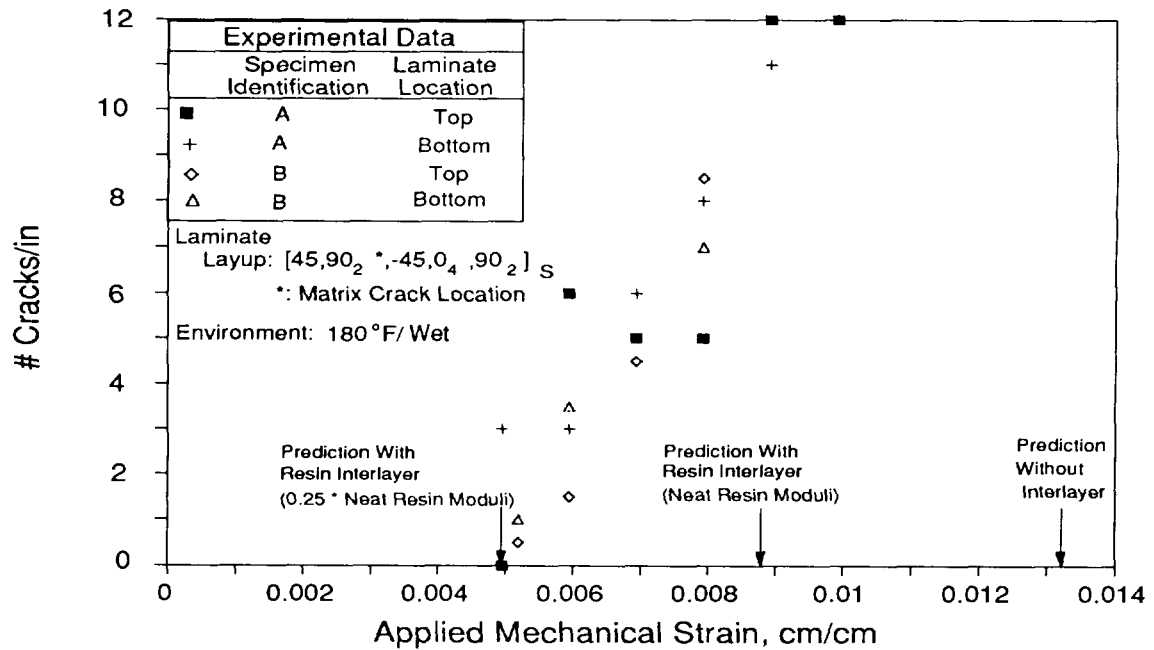


Figure 5. Matrix Crack Onset Predictions and Test Data for a Laminate Exposed to 180°F/Wet.

As mentioned above, the RIL properties used were obtained from measurements of neat resin material. It is likely that the RIL contains preferential amounts of elastomer and other modifiers. Therefore, it is reasonable that environmental conditions will affect the stiffness of the RIL differently than that of the bulk matrix materials in which these agents are interspersed uniformly throughout. Realizing that the assignment of reduced RIL moduli values equal to 25% of the bulk resin was rather arbitrary, the relation between experimental and predicted results indicate that the stiffness of the RIL is probably affected more by environment than was indicated from the neat resin data.

Effects Of Inter- And Intra-laminar Resin Content

A range of mechanical properties were investigated to study the effects of inter- and intra-laminar resin content. Properties of primary interest due to the intended applications of these materials (i.e., fuselage keel panels) were impact damage resistance and tolerance, interlaminar fracture toughness and compressive strength.

Unidirectional Strength and Stiffness: Increasing resin content tends to decrease fiber dominated properties such as unidirectional tensile behavior and compressive stiffness. This was confirmed by experimental results from this study that included different resin distributions (see Table 4). Moduli reported in Table 4 were calculated using the secant between strains of 0.001 in/in and 0.006 in/in. Micromechanics methods (Ref. 18) were used to predict the effect of increasing resin content on lamina axial moduli. Axial tension and compression fiber properties used for these predictions were back-calculated by matching predicted and measured moduli of the baseline material (batch B1). Table 4 shows that micromechanics accurately predicted the effect of decreasing resin content for batches B2, B3, and B4. The experimental tensile failure strains were unaffected by resin content. Since areal weights were held constant in this study, ultimate tensile loads were also unaffected and failure stresses were inversely proportional to specimen thickness.

Material Batch	Tensile Modulus		Ultimate Tensile		Compressive Modulus	
	Measured (Msi)	Predicted (Msi)	Strength (Ksi)	Strain (in/in)	Measured (Msi)	Predicted (Msi)
B1	21.6	21.6	384	0.0163	18.3	18.3
B2	19.9	20.0	350	0.0164	16.8	17.0
B3	19.9	20.0	351	0.0163	17.0	17.0
B4	18.5	18.5	318	0.0159	15.5	15.7

Table 4 - Fiber Dominated Properties For Resin Content Study (Average of Five Specimens)

Flexural stiffnesses (determined while performing end notch flexure tests for fracture toughness) for unidirectional specimens with equal numbers of plies increased as a squared function of per ply thickness. This resulted from the moment of inertia increasing as a cubed function of thickness while the modulus decreased approximately as the inverse of per ply thickness. Changes in flexural stiffness were found to be important in this work for cases involving impact response and sublaminar stability. This will be discussed later.

Ultimate compressive strength properties were observed to be influenced by resin content. Materials displayed higher ultimate compressive loads and failure strains with increasing resin contents. Table 5

shows results that are the average of five specimens per batch. Failure strains were calculated by dividing the measured ultimate strength by measured compression moduli listed in Table 4.

Material Batch	Failure Load, lb (Stand. Dev.)	Ultimate Strength, Ksi (Stand. Dev.)	Failure Strain (in/in)	Specific Strength, in. σ_{ult}/ρ
B1	9400 (227)	207.4 (5.8)	0.0113	3.62×10^6
B2	9876 (765)	200.8 (16.3)	0.0119	3.55×10^6
B3	9904 (626)	200.5 (14.5)	0.0118	3.54×10^6
B4	10,538 (350)	195.5 (7.2)	0.0126	3.50×10^6

Table 5. Ultimate Compressive Properties From Resin Content Study: Unidirectional IITRI Specimens

Unlike the tensile case, increased compressive failure strains were measured for samples with increased resin content. One unidirectional compression specimen (IITRI) from each batch was strain gaged and the load-strain curves from these specimens are given in Figure 6. The observed trends of increasing ultimate compressive strain with increased resin content agree qualitatively with the analysis of Reference 10. To date, experimental results in Table 5 have not been quantitatively compared to predictions based on this analysis.

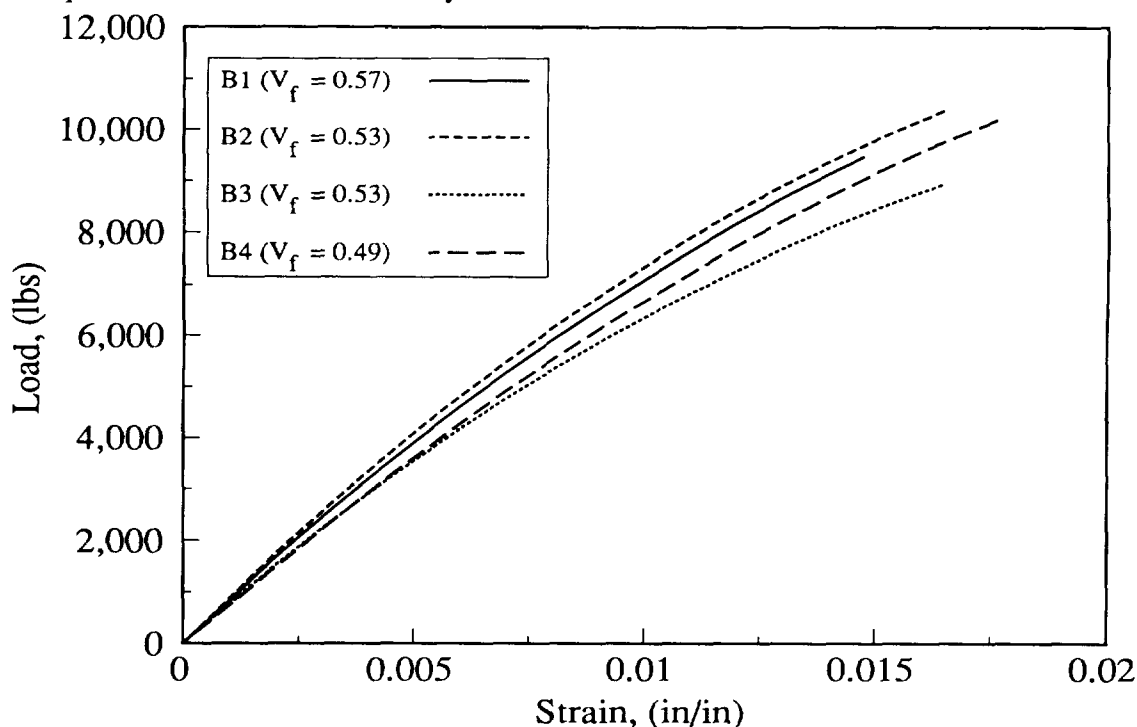


Figure 6. Compressive Load Versus Strain Curves for Samples From Each Batch in the Resin Content Study

Improvements in compression performance are also noted by other columns in Table 5. Increases in compressive failure loads with increasing resin content reported in Table 5 are greater than would be expected due to the added specimen thickness (i.e., load carrying capability of the additional resin). For instance, the additional resin for specimens from batch B4 (highest resin content) carry approximately 60 lb more than batch B1 (lowest resin content) at a failure strain of 0.013 in/in. A far greater incremental increase in ultimate load was observed for these tests. In order to compare the results on a per weight basis, specific compressive strengths (ultimate strength/density) were calculated for each batch. As shown in Table 5, the decreasing density due to increased resin content nearly counteracted the increased thickness (and hence specimen weight) in the specific strength calculation.

Open Hole Compression Strength: A similar influence of resin content was found in results from open hole compression tests. These results are shown below in Table 6. These results were obtained from face supported open hole specimens. The relative increases in failure loads with increasing resin content were approximately the same as for the unidirectional results. Results from face supported quasi-isotropic compression specimens without holes are also included in Table 6. Results from the specimens with no holes did not show the same ordering of the batches as did the specimens with holes. The results from specimens without holes also showed greater scatter than those with holes.

Hole Diameter (in)	BATCH							
	B1		B2		B3		B4	
	Load (Kips)	Strength (Ksi)						
No Hole	11.6	84.0	11.0	72.7	11.0	72.4	12.2	74.7
1/8"	7.1	51.2	7.5	49.6	7.4	48.4	7.8	48.0
1/4"	5.9	42.7	6.4	42.2	6.3	41.4	6.6	40.5
1/2" ¹	4.9	35.5	5.3	34.5	5.3	34.3	5.5	33.9

Notes:¹ 1/2 in. diameter OHC specimens were 2.5" wide compared to 1.5" width with other hole sizes. Failure loads reported were adjusted by the ratio of the widths for comparison purposes.

Table 6. Open Hole Compression Results For Resin Content Study

Interlaminar Fracture Toughness: Table 7 lists the critical mode I (G_{IC}) and mode II (G_{IIC}) interlaminar strain energy release rates that were obtained for the four batches of Toray material. Mode I fracture specimens were given a mode I precrack from an FEP insert prior to testing, and mode II specimens were given a mode II precrack. Mode I results were calculated using the area method. Mode II values were calculated using the beam theory solution corrected for shear (Ref. 14). Shear corrections were between 4 and 6% for the specimens tested. Note that comparisons between G_{IIC} values given in Figure 1 for IM7/8551-7 and those listed for T800/3900-2 in Table 7 should be made with caution, as the former were obtained using mode I precracks. In many cases, G_{IIC} values obtained using mode I precracks are significantly lower than those obtained with mode II precracks.

Values of average RIL thickness were measured experimentally from photomicrographs of polished cross sections. Both unidirectional and quasi-isotropic specimens were used for RIL thickness measurements. The values reported in Table 7 are the average of approximately 45 measurements of RIL thickness for each batch.

Experimental results in Table 7 show that G_{IIC} increases with interlaminar resin content and RIL thickness. Values of G_{IC} were only minimally affected by resin content and distribution. Figure 7 shows a plot of G_{IIC} versus RIL thickness for the four batches. Also shown on Figure 7 are trend lines for similar experiments conducted in Reference (6) with adhesive layers between aluminum adherends. Data from the current work falls in a similar range to results from the cited reference.

Material Batch	G_{IC} (in-lb/in ²)	G_{IIC} (in-lb/in ²)	RIL THICKNESS (10 ⁻³ in)
B1	1.43	10.7	0.6
B2	1.48	12.1	0.7
B3	1.39	12.8	0.7
B4	1.41	13.2	0.9

Table 7. Interlaminar Fracture Toughness For Resin Content Study

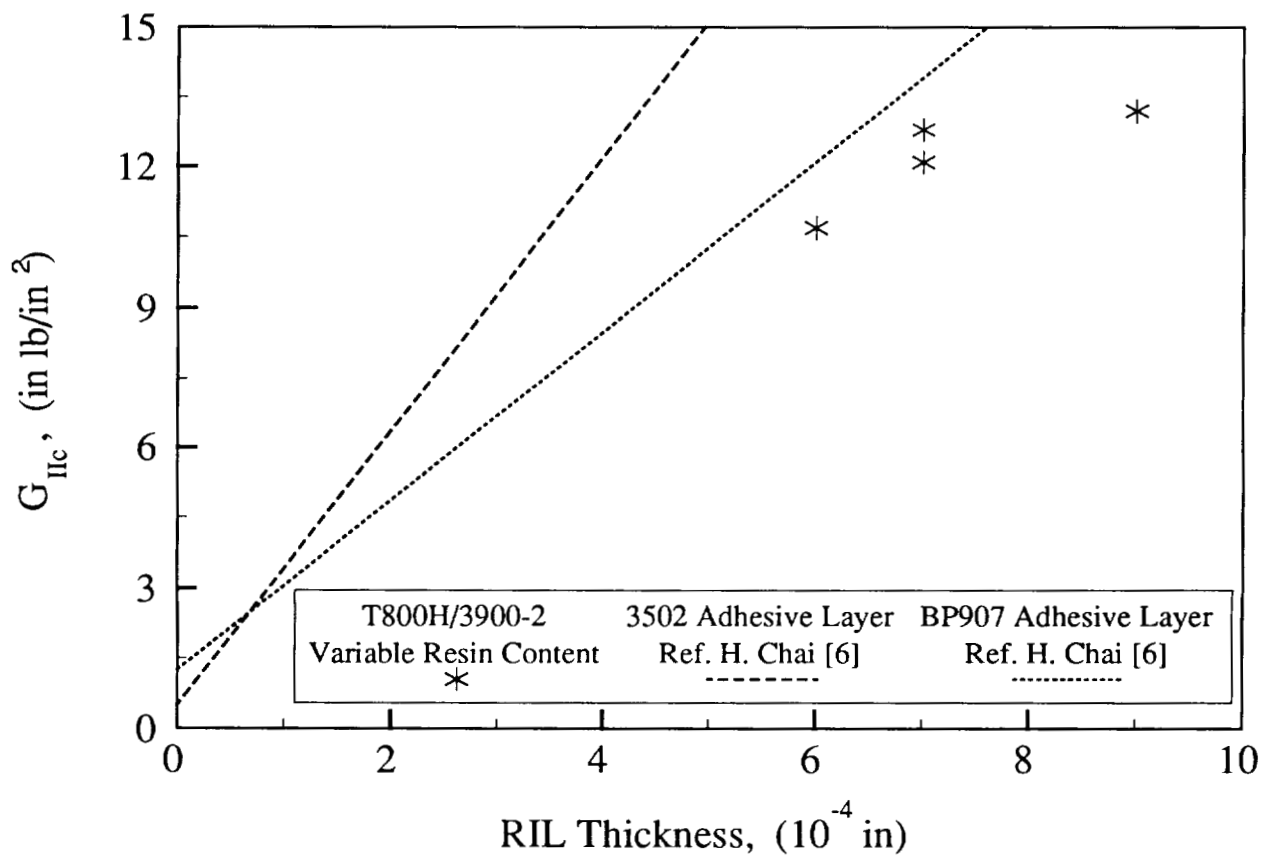


Figure 7. Average RIL Thickness Effects on G_{IIC} for Various Matrices.

It is interesting to note that although the target interlaminar resin contents were different for Batches B2 and B3, the experimental measurements of RIL thickness did not detect differences between these batches. This may indicate that some redistribution of the constituents occurs during cure, and may indicate a limit to the precision with which the RIL lamina architecture may be achieved.

Impact Damage Resistance: The study of composite impact damage resistance is complex due to interactions of materials properties, competing failure mechanisms, structural variables and impact geometry. General analysis tools to predict the formation of impact damage currently do not exist. In some instances, when groups of specimens display behavior that is sufficiently self-similar, relationships can be developed between materials properties and damage resistance. One example of such a case is given in Figure 8 for IM7/8551-7 showing the relationship between mode II interlaminar toughness and damage area for CAI specimens impacted at energies of 270 in.-lb. The corresponding plot of CAI strength versus mode II toughness was given in Figure 1.

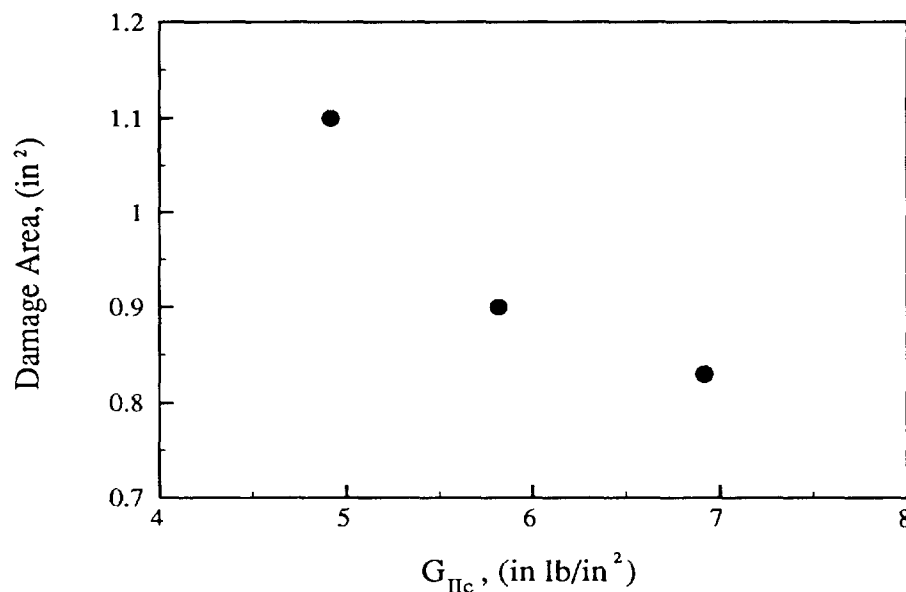


Figure 8. Relationship Between Impact Damage Area and G_{IIc} for IM7/8551-7

The relationships shown in these figures are dependent upon obtaining a degree of similarity in the damage for each case. For the data shown in Figures 1 and 8 the damage zones were dominated by sublaminates formed by impact induced delaminations (Ref. 9). Such relationships in damage resistance and tolerance may break down if a change in the dominant damage mechanism occurs. For instance, different material parameters influence the formation of competing failure mechanisms such as delaminations and fiber breaks. In addition, the post impact response (damage tolerance) is different for delamination and fiber failure dominated damage zones (Ref. 15). Simple relationships may also break down due to differences in the dynamics of the impact event. For example, changes in structural variables such as panel thickness can affect the stress fields that occur during impact.

Past work has indicated that higher values of G_{IIc} tend to increase impact damage resistance and CAI in standard CAI coupon tests. As discussed earlier, experimental values of G_{IIc} increased with increasing resin content in the current study. The higher resin contents also led to greater panel thickness, and hence increased flexural stiffness. The net effect of increased resin content on impact damage resistance is shown in Figure 9 for the four batches tested. As can be seen from these results, damage area tended to be greater for the higher resin content batches. This seems to indicate that the increased specimen thickness associated with higher resin contents more than offsets the increased toughness. Methods to scale results from impact events with varying panel sizes have been reported in the literature (e.g., Ref. 16); however, the simultaneous changes in important material and structural variables for specimens in the current work complicates such an approach.

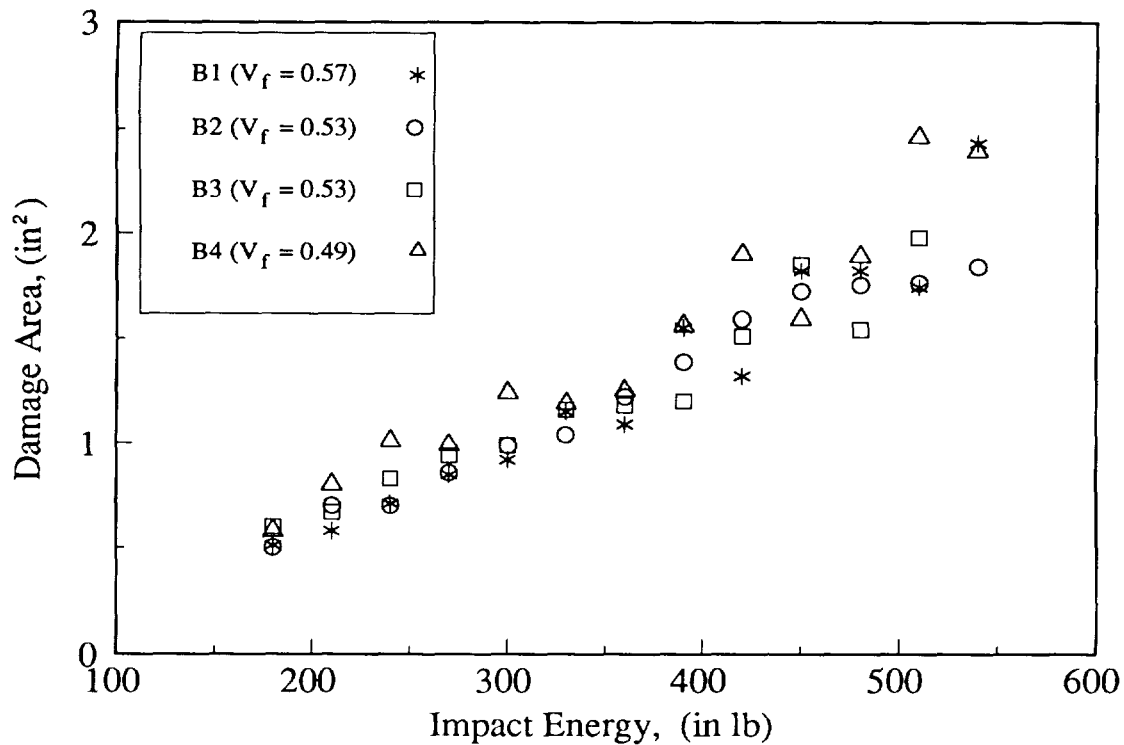


Figure 9. Damage Resistance Results for Resin Content Study

Impact response of the CAI panels was studied experimentally and analytically in order to develop further understanding of this behavior. Impacting was performed using an instrumented impact tower which recorded force-time data at the rate of 40 data points per millisecond for the first 24 milliseconds of the impact events. Force-time, force-displacement and energy-time curves were reduced from these data. Predictions of the elastic impact response of test coupons used a series solution for a laminated composite plate subjected to low velocity impact (Ref. 17). Transverse shear is included in this analysis. The analysis provides force-time and displacement-time predictions for the impact event, as well as stress and strain distributions. The required lamina properties which were not measured experimentally (e.g., E_{22} , G_{12}) were determined from a combination of results from existing databases for the baseline material and calculations using micromechanics (Ref. 18).

Figure 10 shows experimental force-time curves for batches B1, B2 and B4 subjected to a 180 in-lb impact. Results are not presented for B3 since B2 and B3 displayed very similar impact response. The overall resin contents were identical for batches B2 and B3 and thus the panel thicknesses and flexural stiffnesses were essentially the same. As shown in Figure 10, higher peak loads and faster load response were obtained from the batches with increased resin content. This reflects increases in flexural stiffness due to greater specimen thickness. Maximum loads measured experimentally during the impact event varied by 7.5% between batches with the highest and lowest resin content. Elastic analysis predicted a 12% difference indicating the greater driving force for damage formation due to increased specimen thickness.

Figure 11 shows analytical and experimental results for a specimen from batch B4 impacted at 180 in-lb. The 180 in-lb impact was the lowest impact energy studied in this work. As mentioned above, the analysis is for elastic behavior and does not include local loss of stiffness due to damage accumulation. The model corresponds well with the experimental results for times of less than

approximately 1 millisecond. The deviation of curves at times greater than 1 millisecond is hypothetically due to the development of damage in the panel. Thus, the analytical model was used as a benchmark from which to judge the onset of damage. Damage onset loads determined by comparison of the experimental and analytical data as outlined above were 1929 lb, 2094 lb, and 2400 lb for batches B1, B2, and B4, respectively (24% difference between B1 and B4). This appears to relate to increases in G_{IIc} . Any additional correlations would require the formulation of an analytical model to predict the net effect of the competing material and structural variables.

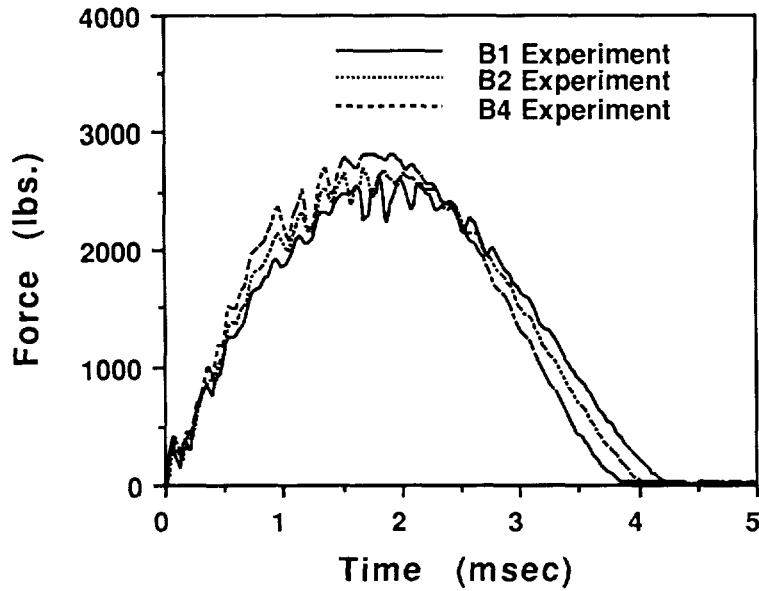


Figure 10. Instrumented Impact Results for the Resin Content Study

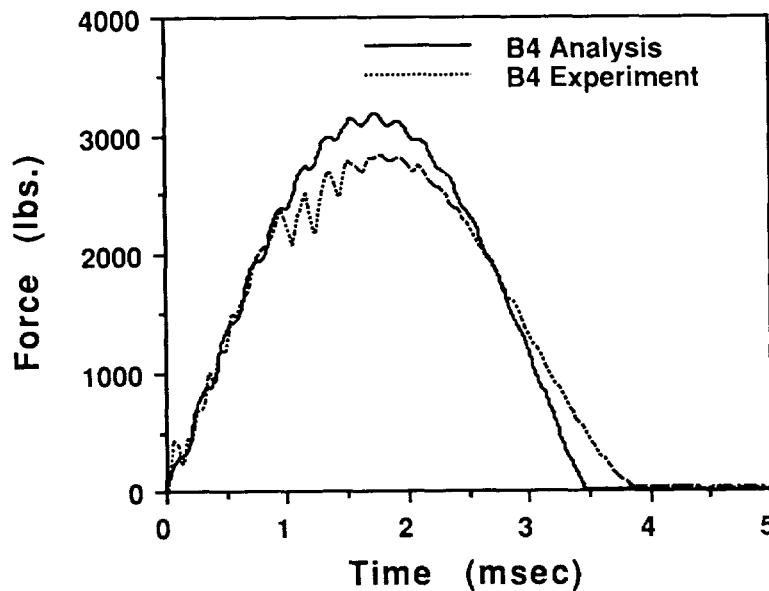


Figure 11. Predicted and Experimental Results for a Specimen from Batch B4, Impacted at an Energy of 180 in-lb.

Competing Failure Mechanisms: Damage mechanisms which are operative during the impact event include delamination, intraply matrix cracking and fiber failure. The relative occurrence of these mechanisms varies with structural configuration, material properties, impact energy, and impactor geometry. Complex interactions between various damage mechanisms contribute to the challenges involved in modeling impact damage resistance of composite materials.

The intraply matrix cracking and delamination which contribute to the formation of a characteristic damage state for the quasi-isotropic CAI specimen has been well documented (e.g., Ref. 9). Delaminations are connected by intralaminar cracks to form a spiral staircase configuration of sublaminates. The relative ratio with which these two mechanisms occur can vary depending on the balance of material properties (Ref. 4). Matrix cracking and interlaminar fracture studies discussed earlier indicated differing relationships with the RIL. The increase in interlaminar G_{IIc} and decrease in in situ strengthening with greater RIL thickness would be expected to favor intralaminar matrix cracking over delamination as a mode for dissipating impact energy. Further work will be performed to study the relative contributions of delamination and matrix cracks to the impact damage state. Clearly, the latter is expected to have less of an effect on CAI.

The TTU method was used to obtain a measurement of the damage area as viewed in the plane of the panel. This has proved to be a useful measure that quantifies the size of known characteristic damage states for CAI analysis. Visible indications of impact damage are also important, both for in-service detection of damage and to identify failure mechanisms. The visible damage documented in this work included dent depth measurements and surface damage descriptions (front and back).

Dent depth measurements are shown in Figure 12 as a function of impact energy for the lowest (B1) and highest (B4) resin content batches. Dent depths were greater for a given impact level in the lower resin content materials. Other visible indications of damage, such as fiber breakage on the front and back surfaces of impacted panels, were also observed to occur at lower energy levels for the lower resin content materials. Local damage mechanisms under the point of impact which lead to visible damage indications are thought to be dominated by fiber failure. It is likely that changes in sublaminate thickness between different material batches affect the ratio of local fiber failure and delamination that occurs.

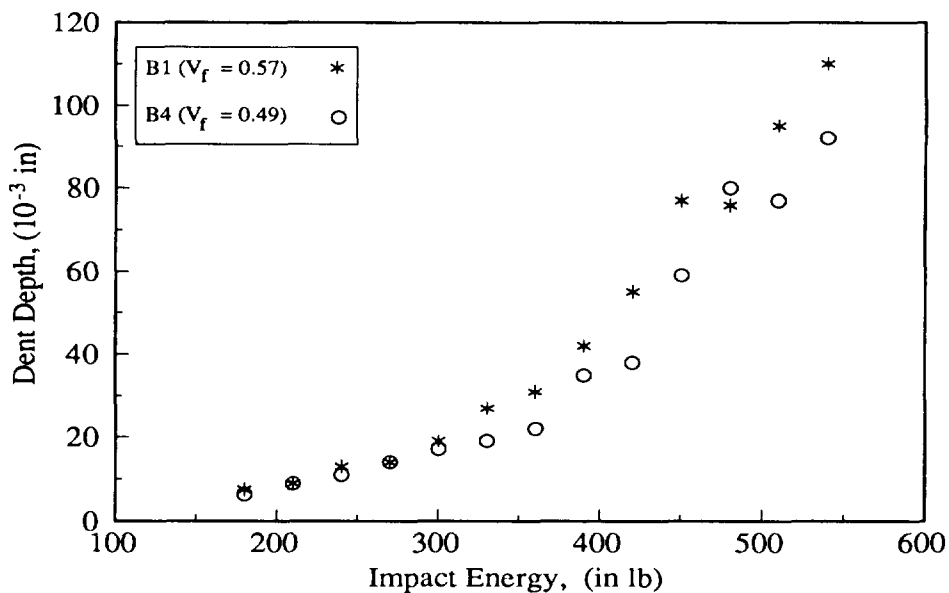


Figure 12. Experimental Measurements of Impacted Surface Damage

Figure 13 shows TTU measurements of damage area plotted versus dent depth for batches B1 and B4. The higher resin content materials, which also had the greatest sublaminate thickness, had larger delamination for a given dent depth. Measurements of the elastic rebound of the impactor indicated that a greater amount of energy was absorbed in tests involving lower resin content materials. This is consistent with increased fiber breakage in these materials. More work is needed to clarify the role of fiber failure in impact damage development.

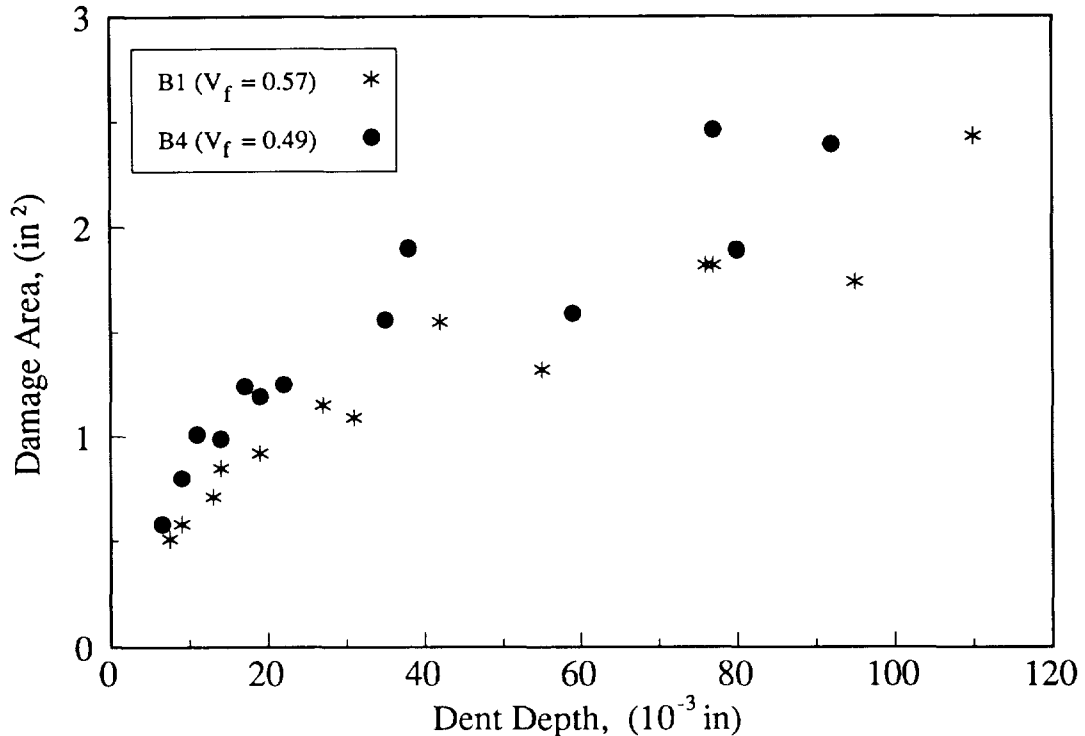


Figure 13. Measurements Relating Delamination Area and Surface Damage

Damage Tolerance: Damage tolerance was investigated using the 4 in. by 6 in. CAI coupon test. Figure 14 shows experimental failure strains versus damage area for the four batches of Toray material. The higher resin content materials exhibit greater failure strains for a given damage size. Since the moduli are lower for higher resin contents, the CAI results for the four batches of material very nearly superposed when plotting failure stress versus damage area.

Results of the CAI tests were compared with predictions obtained using a sublaminate stability analysis described in Reference 9 with good success. This approach has shown good agreement with past experimental data for damage sizes in the range of 1 inch diameter and greater. The model redistributes load in the neighborhood of buckled sublaminates, and then predicts failure due to the effect of this discontinuity. The load carried by sublaminates is assumed to be constant following buckling. Final failure is predicted due to compressive failure at the boundary of damaged and undamaged material. Experimental measurements of compression moduli (Table 4) and compressive failure strains (Table 5) were used in CAI analysis. Per ply thicknesses used in the model were also experimentally determined for the four batches. Other lamina properties required for the analysis were calculated using existing data for batch B1 and micromechanics (Ref. 18) for the three different resin contents.

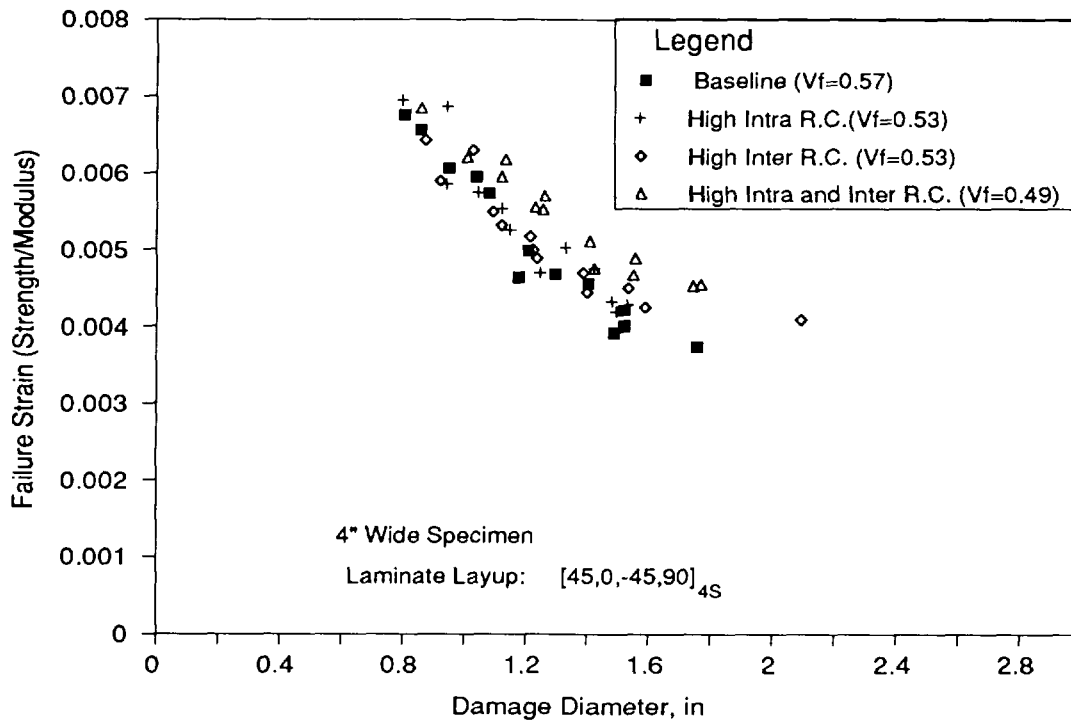


Figure 14. Damage Tolerance Results for the Resin Content Study

Plots of predicted and experimentally determined CAI strengths are shown in Figures 15, 16, and 17. Results for batches B2 and B3 are superposed in Figure 16 because analysis results were equivalent for materials having the same overall resin content. The comparison between theory and experiment is excellent for each case.

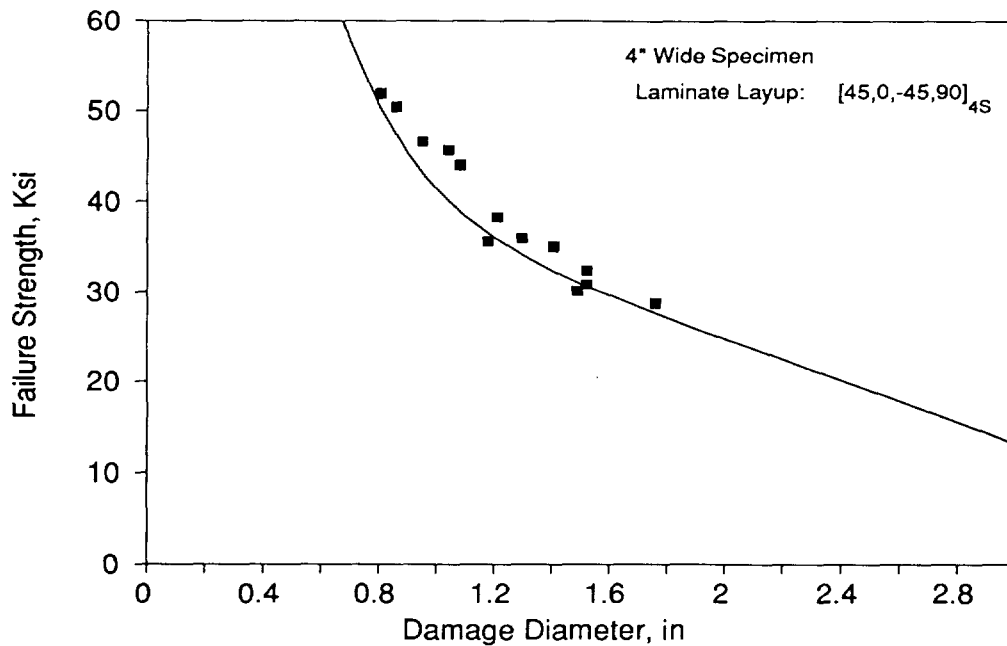


Figure 15. Damage Tolerance Analysis and Test for Batch B1.

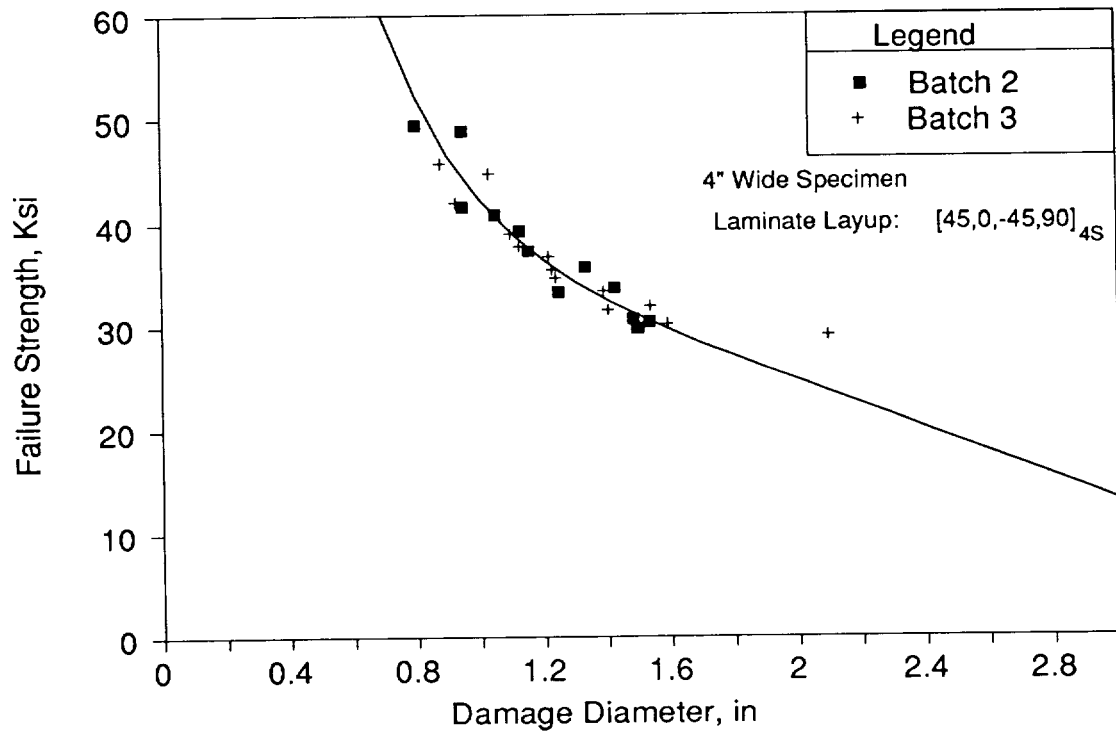


Figure 16. Damage Tolerance Analysis and Test for Batches B2 and B3.

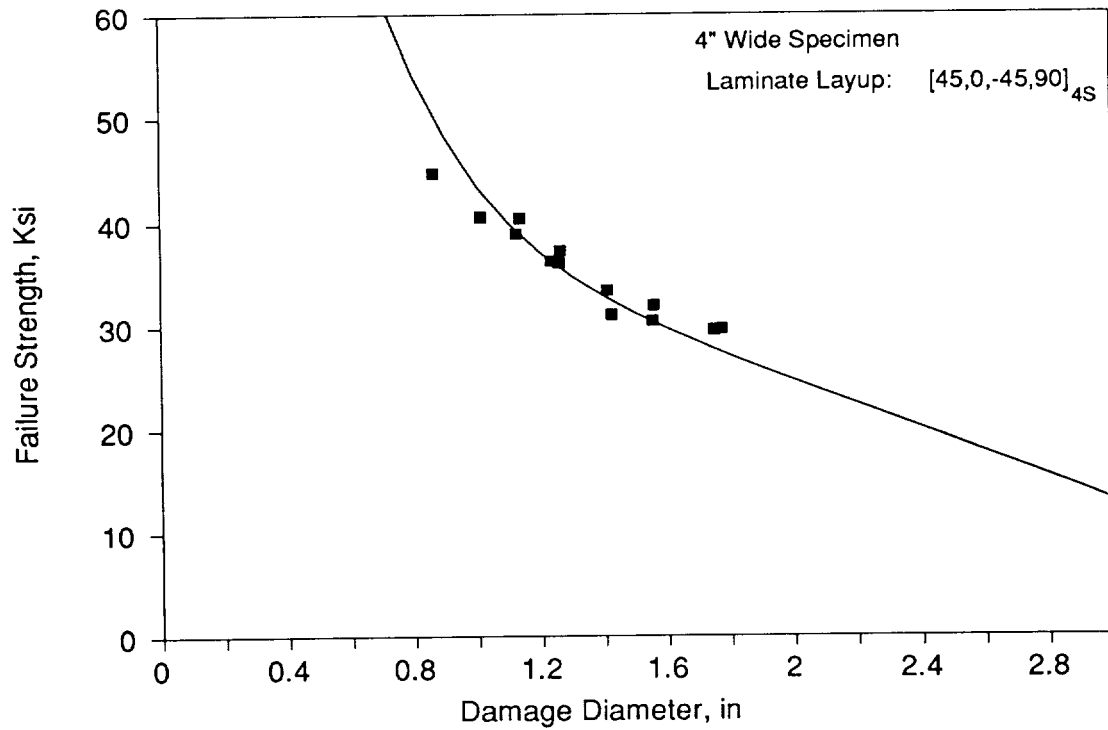


Figure 17. Damage Tolerance Analysis and Test for Batch B4.

A slight deviation was observed between theory and experiment from the highest resin content batch (see Figure 17) for small damage sizes. This is believed to be due to the greater stability of the thicker sublaminates. At small damage sizes, the thicker sublaminates have a greater relative stability and the effect of other impact damage such as fiber failure increases. This deviation of the experimental data from the predicted trend has been noted in past work for materials with per ply thicknesses of greater than 0.007 in. (Ref. 19). The lower resin content materials which have thinner sublaminates comprising their damage zone reflect trends dominated by stability for smaller damage diameters.

ECONOMIC CONSIDERATIONS

Cost and weight trades need to be considered when evaluating the merits of increased resin content. Resin can cost as much as an order of magnitude less than fiber. As a result, the performance value associated with lower material costs may offset marginal increases in weight. Increased resin content may also yield a more robust material for processing (e.g., minimize the void content of complex laminate geometries). If increased resin content results in thicker plies, as in the current study, additional benefits are possible by attaining the required structural thickness with reduced ply layup labor costs. Since flexural stiffness is enhanced with increasing ply thickness, stability performance trades would likely favor increased resin content. The current study provides an example in which damage tolerance is also favorably influenced by increased ply thickness and greater compressive failure strains associated with higher resin contents.

Additionally, approaches have been proposed in which discrete layers of adhesive are selectively placed between plies in areas requiring enhanced interlaminar shear properties. If the performance penalty for uniformly increasing the RIL thickness is small, the economics may favor a uniform RIL rather than adding additional process steps for selectively inserting the adhesive layers. A need for additional interlaminar resin may be required in applications involving considerable amounts of interlaminar load redistribution. Several examples exist for a transport fuselage; including, (1) doubler plies near door and window cutouts, (2) laminate thickness tailoring in keel panels near the keel beam for the redistribution of large compressive loads. The effects of increased resin content on compressive load redistribution in the neighborhood of ply drop-offs will be the subject of additional studies under Contract NAS1-18889.

CONCLUSIONS

Several mechanical properties were evaluated for toughened materials having resin-rich interlaminar layers (RIL). The studies included variations in intra- and inter-laminar resin content. Results indicate that materials with RIL may be favored for applications dominated by compressive loads and interlaminar shear. The keel area of a transport fuselage (i.e., lower portion of the fuselage near the wing-to-body intersection) is one such application. Economic benefits were identified for increased resin content materials. In addition to lower raw material cost, high resin content materials may be more robust for manufacturing. The use of thicker plies in coordination with higher resin content could also reduce layup costs.

The influence of RIL architecture on matrix cracking was investigated with the help of experiments and analysis. The RIL decreased the in-situ transverse strengthening effect noted in past composite studies. Comparisons of analytical and experimental results indicate that matrix crack predictions could be off by more than a factor of two if the effects of RIL and environmental are not adequately simulated.

Increased resin content in RIL materials had little or no benefit for fiber dominated properties such as axial moduli. Changes in axial tension and compression moduli with increasing resin content were accurately predicted by micromechanics methods. The flexural stiffness of high resin content samples increased, despite lower moduli, due to the increased ply thickness.

Compressive failure strains increased with increasing resin content. For example, an 8% by weight addition of resin increased the compressive failure strains of unidirectional specimens by 12%. Similar increases in open-hole compression failure strains were also observed. These results agree qualitatively with the compressive behavior predicted by the model of (Ref. 10).

The increased resin content in the form of an RIL was found to increase mode II interlaminar toughness. The critical mode II interlaminar strain energy release rate was observed to increase 23% due to the addition of 8% by weight of resin. Mode I interlaminar toughness was not affected by resin content in this study.

Higher mode II toughness did not translate to increased impact damage resistance in standard coupon tests. This was due to interactions with structural variables (e.g., increased panel thickness and flexural stiffness) which increased the severity of the impact event for high resin content samples. In the absence of such effects, the increased mode II toughness would be expected to confer improved damage resistance to impact stresses dominated by interlaminar shear.

Visible damage (dent depth and surface fiber breakage) at a given impact energy was greatest for the thinnest specimens (i.e., lower resin content materials). This, combined with the larger delamination areas for the thickest specimens (i.e., high resin content materials), led to a larger ratio of visible to invisible damage for the relatively thin specimens. This reflects differing contributions from the various damage mechanisms which depend on structural variables as well as material properties.

Compression failure strains for a given damage diameter were improved for CAI coupons with higher resin contents. Analytical predictions based on a sublaminar stability approach agreed well with the experimental CAI data for all resin contents. Model variables identified as playing a key role in increasing CAI for higher resin content materials were sublaminar stability and undamaged failure strains. The influence of increased sublaminar stability is apparent in CAI failure strain curves for small damage sizes, while the influence of increased undamaged compressive failure strain is reflected at the larger damage sizes.

ACKNOWLEDGMENTS

The authors would like to acknowledge Toray Industries, Inc. and M. Katsumoto for providing the special resin content materials used in this study. We would also like to thank J. McCool for experimental support.

REFERENCES

1. Masters, J.E., "Characterization of Impact Damage Development in Graphite/Epoxy Laminates," Fractography of Modern Engineering Materials, ASTM STP 984, ASTM, Philadelphia, 1987, pp. 238-258.
2. Evans, R.E., and Masters, J.E., A New Generation of Epoxy Composites for Primary Structural Applications: Materials and Mechanics," Toughened Composites, ASTM STP 937, ASTM, Philadelphia, 1987, pp. 413-435.

3. Ilcewicz, L.B., Dost, E.F., McCool, J.W., and Grande, D.H., "Matrix Cracking in Composite Laminates with Resin Rich Interlaminar Layers, Presented at 3rd Symposium on Composite Materials: Fatigue and Fracture, Nov. 6-7, Buena Vista, Fla., ASTM, 1989.
4. Grande, D.H., and Schaffnit, R.S., "Materials Parameters and Mechanisms Associated with Toughening and Compression After Impact Behavior of Composite Materials," Presented at 2nd Topical Conference on Emerging Technologies in Materials, Nov. 6-9, 1989, San Francisco, American Institute of Chemical Engineers.
5. Recker, H.G., et. al., "Toughened Thermosets for Damage Tolerant Carbon Fiber Reinforced Composites," SAMPE Journal, Vol. 26, No. 2, March/April 1990, pp. 73-78.
6. Chai, H., "Shear Fracture", International Journal of Fracture, Vol. 37, 1988, pp. 137-159.
7. Sela, N., Ishai, O., and Bank-Sills, L., "The Effect of Adhesive Thickness on Interlaminar Fracture Toughness of Interleaved CFRP Specimens," Composites, Vol. 20, No. 3, May 1989, pp. 257-264.
8. Chai, H., "Interlaminar Shear Fracture of Composites," International Journal of Fracture, Vol. 43, 1990, pp. 117-131.
9. Ilcewicz, L.B., Dost, E.F., and Coggeshall, R.L., "A Model for Compression After Impact Strength Evaluation," Proc. 21st International SAMPE Technical Conf., 1989, pp. 130-140.
10. Shuart, M.J., "Short-Wavelength Buckling and Shear Failures for Compression-Loaded Composite Laminates," NASA Technical Memorandum 87640, National Aeronautics and Space Administration, Nov. 1985.
11. Shuart, M.J., "Failure of Compression-Loaded Multi-Directional Composite Laminates," AIAA Paper No. 88-2293, Presented at the AIAA/ASME/ASCE/AHS 29th Structures, Structural Dynamics and Materials Conference, Williamsburg, VA, April, 1988.
12. Coxon, B.R., Walker, T.H., Ilcewicz, L.B., and Seferis, J.C., Proc. of Spring SEM Conf., Society for Experimental Mechanics, 1987.
13. Coquill, S.L., and Adams, D.F., "Mechanical Properties of Several Neat Polymer Matrix Materials and Unidirectional Carbon Fiber Reinforced Composites," NASA CR-181805, National Aeronautics and Space Administration, April, 1989.
14. Carlsson, L.A., Gillespie, J.W. Jr., and Pipes, R.B., "On the Analysis and Design of the End Notched Flexure (ENF) Specimen for Mode II Testing," J. Comp. Mat., Vol. 20, 1986, p. 594.
15. Cairns, D.S., "Impact and Post-Impact Response of Graphite/Epoxy and Kevlar/Epoxy Structures," PhD Dissertation, Massachusetts Institute of Technology, 1987, (TELAC Report #87-15).
16. Quian, Y., Swanson, S.R., Nuismer R.J., and Bucinell, R.B., "An Experimental Study of Scaling Rules for Impact Damage in Fiber Composites," Journal of Composite Materials, Vol. 24, May 1990, pp. 559-570.
17. Dobyms, A.L., and Porter, T.R., "A Study of the Structural Integrity of Graphite Composite Structures Subjected to Low Velocity Impact," Polymer Science and Technology, Vol. 21, No. 8, 1981, pp. 493-498.
18. Chamis, C.C., "Simplified Composite Micromechanics Equations for Hygral, Thermal and Mechanical Properties," NASA TM-83320, National Aeronautics and Space Administration, Feb. 1983.
- 19.) Dost, E.F., et al, "The Effects of Stacking Sequence On Impact Damage Resistance and Residual Strength for Quasi-Isotropic Laminates," Presented at 3rd Symposium on Composite Materials: Fatigue and Fracture, Nov. 6-7, Buena Vista, Fla., ASTM, 1989.